PHYSICAL REVIEW D VOLUME 49, NUMBER 7 1 APRIL 1994

Nature of the thermal phase transition with Wilson quarks

Claude Bernard
Department of Physics, Washington University, St. Louis, Missouri 63130

Thomas A. DeGrand and A. Hasenfratz
Physics Department, University of Colorado, Boulder, Colorado 80309

Carleton DeTar
Physics Department, University of Utah, Salt Lake City, Utah 84112

Steven Gottlieb
Department of Physics, Indiana University, Bloomington, Indiana 47405
and Department of Physics, Bldg. 510A, Brookhaven National Laboratory, Upton, New York 11973

Leo Kärkkäinen and D. Toussaint
Department of Physics, University of Arizona, Tucson, Arizona 85721

R. L. Sugar
Department of Physics, University of California, Santa Barbara, California 93106
(Received 27 October 1993)

We describe a series of simulations of high temperature QCD with two flavors of Wilson quarks aimed at clarifying the nature of the high temperature phase found in current simulations. Most of our work is with four time slices, although we include some runs with six and eight time slices for comparison. In addition to the usual thermodynamic observables, we study the quark mass defined by the divergence of the axial vector current and the quark propagator in the Landau gauge. We find that the sharpness of the $N_t=4$ thermal transition has a maximum around $\kappa=0.19$ and $6/g^2=4.8$.

PACS number(s): 12.38.Gc, 11.15.Ha

I. INTRODUCTION

Lattice simulations are an important source of information on the behavior of quantum chromodynamics at high temperature. Most work has been done with Kogut-Susskind quarks because of the exact remnant of chiral symmetry. Since the exact chiral symmetry of Kogut-Susskind quarks is a U(1) symmetry, there is some question about how well the results reproduce the real world with its SU(2) chiral symmetry. In the continuum limit the complete chiral symmetry is restored. However, in the continuum limit the results should be independent of the regularization used for the quarks. To test this it is important to study high temperature QCD with the other common form of lattice quarks, the Wilson quarks.

The first simulations of high temperature QCD with two flavors of Wilson quarks revealed a potential problem—for the values of $6/g^2$ for which most low temperature simulations were done, $4.5 \le 6/g^2 \le 5.7$, the high temperature transition occurs at a value of quark hopping parameter κ for which the pion mass measured at zero temperature is quite large [1,2]. In other words, it is difficult to find a set of parameters for which the temperature is the critical temperature and the quark mass is small. Further work confirmed that the pion mass is large at the deconfinement transition for this range of $6/g^2$ [3,4]. (A recent study has concluded that for four time slices the chiral limit is reached at a very small value of $6/g^2 \approx 3.9$ [5].)

Screening masses for color singlet sources show an approach to parity doubling in the high temperature phase similar to what is seen with Kogut-Susskind quarks [2,3]. Also, measurements of the pion mass show a shallow minimum at the high temperature transition [6].

Previous simulations with Wilson fermions have located κ_t, the value of the hopping parameter at which the high temperature crossover or phase transition occurs, as a function of $6/g^2$ for $N_t=4$ and 6. The critical value of the hopping parameter, κ_c, for which the pion mass vanishes at zero temperature has been located with somewhat less precision [1,2,6,7,3,4]. Some measurements of hadron masses have been carried out on zero temperature lattices for values of κ and $6/g^2$ close to the κ_t curve, allowing one to set a scale for the temperature, and to estimate κ_c in the vicinity of the thermal transition [3,4,8].

In more recent work at $N_t=6$ we have observed coexistence of the low and high temperature phases over long simulation times, and we have extended these observations in the present project. The change in the plaquette across the transition is much larger than for the high temperature transition with Kogut-Susskind quarks [4]. This unexplained behavior, as well as work by Hasenfratz and DeGrand on the effect of heavy quarks [9], has led us to extend our work.

 ©1994 The American Physical Society

This paper reports on a series of simulations with Wilson quarks at high temperature, in which we have studied a number of indicators for the nature of the phases. Using $8^3\times4$ lattices, we have extended earlier studies of the location of the thermal transition or crossover to $\kappa=0.20$, 0.21, and 0.22. In the range of $6/g^2$ and κ that have been studied earlier, we have done extensive simulations on $8\times8\times20\times4$ lattices, with additional work on $12^3\times6$, $12^2\times24\times6$, and $8^2\times20\times8$ lattices. For one value of $6/g^2$ we made a series of runs on $6\times6\times20\times4$ lattices to make sure that the effects we see are not due to the spatial size of the lattice. In this article we will concentrate on the results with four time slices. Simulations with $N_t=6$ and 8 are still underway and will be described later.

We see a number of inexplicable effects. At large β and small κ the crossover from the confined phase to the high temperature phase is smooth. Beginning at $(\beta,\kappa)=(5.1,0.16)$ and extending down to about $(\beta,\kappa)=(4.51,0.20)$ the crossover becomes abrupt, though probably not first order. A rapid crossover is seen in the plaquette, real part of the Polyakov loop, $\bar{\psi}\psi$, the entropy, and the quark mass derived from the axial vector current. For $\beta<4.5,\kappa>0.20$ the transition once again becomes very smooth.

Section II discusses the quantities we measured, and Sec. III summarizes the simulations and the results. Conclusions are in Sec. IV.

II. MEASURED QUANTITIES

In our simulations we have measured the expectation values of the Polyakov loop, the space-space and space-time plaquettes, the chiral condensate $\bar{\psi}\psi$, the entropy, screening masses for meson sources, the quark mass defined by the divergence of the axial vector current, and quark propagators in Landau gauge.

The expectation value of the Polyakov loop, $\langle P\rangle$, is simply interpreted as $\exp(-F_q/T)$, where F_q is the free energy of a static test quark. With dynamical quarks $\langle P\rangle$ is always nonzero, but it increases dramatically at the high temperature transition. We also measured the space-space and space-time plaquettes $\langle\Box_{ss}\rangle$ and $\langle\Box_{st}\rangle$. In our normalization these are equal to three on a completely ordered lattice.

The energy, pressure, entropy, and $\bar{\psi}\psi$ with Wilson quarks are obtained by differentiating the partition function with respect to the temporal size, the spatial size, and the quark mass, respectively. Details are given in the Appendix. We study the entropy to lowest order in g and $\bar{\psi}\psi$, using the formulas

$$\langle\bar{\psi}\psi\rangle=\frac{1}{N_s^3N_t}\frac{4\kappa N_f}{2}\mathrm{Re}\left\langle\mathrm{Tr}\frac{1}{M^\dagger}\right\rangle \tag{1}$$

and

$$\begin{aligned}\langle s_g a^4\rangle\frac{1}{aN_t}&=\frac{1}{3N_s^3N_t}\sum_x\left\langle-\frac{\partial S_g}{\partial\alpha_t}+\frac{1}{3}\frac{\partial S_g}{\partial\alpha_x}+\frac{1}{3}\frac{\partial S_g}{\partial\alpha_y}+\frac{1}{3}\frac{\partial S_g}{\partial\alpha_z}\right\rangle\\&=\frac{1}{N_2^3N_t}\sum_x\left\langle\left[\frac{8}{g^2}+4(C_\tau-C_\sigma)\right](\Box_{st}-\Box_{ss})\right\rangle\end{aligned} \tag{2}$$

and

$$\begin{aligned}\langle s_f a^4\rangle\frac{1}{aN_t}&=\epsilon_f a^4+p_f a^4\\&=\frac{-2}{N_s^3N_t}\frac{\kappa N_f}{2}\mathrm{Re}\left\langle 2\mathrm{Tr}\frac{1}{M^\dagger}\left[\not{D}_0-\frac{1}{3}\sum_i\not{D}_i\right]\right\rangle\end{aligned} \tag{3}$$

where s_g and s_f are the gluon and fermion entropies, respectively.

We measured screening masses for meson sources with quantum numbers of the π, σ, ρ, and a_1. These measurements are a standard hadron spectrum calculation, except that the propagation is in the z direction. We used a wall source covering the entire $z=0$ slice of the lattice, with the gauge fixed to a spatial Coulomb gauge which maximizes the traces of the x, y, and t direction links. After blocking five to ten measurements together to minimize the autocorrelations, we fit all the propagators to a single exponential using the full covariance matrix of the propagator elements.

A quark mass can be defined from the divergence of the axial current [10,11]. The basic relation is a current algebra relation

$$\nabla_\mu\cdot\langle\bar{\psi}\gamma_5\psi(0)\bar{\psi}\gamma_5\gamma_\mu\psi(x)\rangle=2m_q\langle\bar{\psi}\gamma_5\psi(0)\bar{\psi}\gamma_5\psi(x)\rangle\ . \tag{4}$$

If we sum over x, y, t slices, and measure distance in the z direction, this becomes

$$\begin{aligned}\frac{\partial}{\partial z}\sum_{x,y,t}\langle\bar{\psi}\gamma_5\psi(0)\bar{\psi}\gamma_5\gamma_3\psi(x)\rangle&\\=2m_q\sum_{x,y,t}\langle\bar{\psi}\gamma_5\psi(0)\bar{\psi}\gamma_5\psi(x)\rangle\ .&\end{aligned} \tag{5}$$

We define $\Pi(z)$ as the pion correlator with a point sink,

$$\Pi(z)=\langle W(0)\bar{\psi}\gamma_5\psi(z)\rangle \tag{6}$$

and $A(z)$ also the axial vector current correlator:

$$A(z)=\langle W(0)\bar{\psi}\gamma_5\gamma_z\psi(z)\rangle\ , \tag{7}$$

where $W(0)$ is the wall source at $z=0$. At long distances both $\Pi(z)$ and $A(z)$ will fall off as $\exp(-m_\pi z)$. Therefore we perform a simultaneous fit to the two propagators on a lattice periodic in the z direction using three parameters, C, m_π, and m_q:

$$\Pi(z)=C\sinh(m_\pi)\{\exp(-m_\pi z)+\exp[m_\pi(N_z-z)]\}\ , \tag{8}$$

$$A(z)=C2m_q\{\exp(-m_\pi z)-\exp[m_\pi(N_z-z)]\}\ . \tag{9}$$

The factor of $\sinh(m_\pi)$ in Eq. (8) comes from using the lattice difference $f(z+1)-f(z-1)$ for the derivative in Eq. (5). Note that $\Pi(z)$ is periodic in z while $A(z)$ is antiperiodic. We use the pointlike axial vector current $\bar{\psi}(z)\gamma_5\gamma_\mu\psi(z)$ rather than a point split current. These are quark masses in lattice units; to convert to continuum quark masses requires a lattice-to-continuum renormalization. See Ref. [17] for a discussion of this point.

The quark propagator in the Landau gauge was also measured. This propagator has been studied with Kogut-Susskind quarks in Ref. [12]. We chose a source constant in the y direction and a δ function in x, z, and t with only the real part of the first Dirac component nonzero (in the Weyl basis we use). Because of the δ function all possible momenta in x, z, and t directions were excited. To distinguish among the different momenta we performed a Fourier transform of the propagator in x and t directions (taking into account that it has to have odd frequencies in t direction). This gives the propagation of the quark in the z direction as function of k_x and k_t, i.e., the dispersion relation of the screening propagator. In order to keep the amount of generated data at a reasonable level, the propagator was saved only for on-axis momentum values of k_x and k_t. This enabled us to measure the on-axis dispersion relation of the quark screening mass, in particular the screening mass difference of the quark and light doublers.

The form to which the spatial propagator is fitted is usually motivated by the form of the free propagator. We suppose that at large distances, each separate momentum component of the spatial propagator resembles the corresponding free quark form, but with its own renormalized quark mass, or in this case of Wilson fermions, with a renormalized κ.

In momentum space the free Wilson propagator is

$$G(k)=\frac{\left[1-2\kappa\sum_\mu\cos(p_\mu)\right]-i2\kappa\sum_\mu\gamma_\mu\sin(p_\mu)}{\left[1-2\kappa\sum_\mu\cos(p_\mu)\right]^2+4\kappa^2\sum_\mu\sin^2(p_\mu)}\ . \tag{10}$$

With our choice of the source the first Dirac component of the propagator, G_1, is real:

$$G_1=\frac{\left[1-2\kappa\sum_\mu\cos(p_\mu)\right]}{\left[1-2\kappa\sum_\mu\cos(p_\mu)\right]^2+4\kappa^2\sum_\mu\sin^2(p_\mu)}\ . \tag{11}$$

Then, for nonzero z values,

$$\begin{aligned}G(p_1,p_2,z,p_0)&=\sum_{k=1}^{L_z}\exp[i2\pi kz/L_z]G(p_1,p_2,k,p_0)\\&=L_z\left[\frac{(1-6\kappa+4\kappa A)^2-4\kappa(B+1)}{8\kappa(1-6\kappa+4\kappa A)^2}\right]\\&\quad\times\left[\frac{\cosh[ma(z-L_z/2)]}{\sinh(ma)\sinh(maL_z/2)}\right]\ ,\end{aligned} \tag{12}$$

where

$$A=\sum_{\mu=1,2,0}\sin^2[p_\mu/2]\ , \tag{13}$$

$$B=\sum_{\mu=1,2,0}\sin^2[p_\mu]\ , \tag{14}$$

and

$$ma=2\,\mathrm{arcsinh}\left[\frac{4\kappa^2B+(1-8\kappa+4\kappa A)^2}{8\kappa(1-6\kappa+4\kappa A)}\right]^{1/2}\ . \tag{15}$$

At zero momentum (on a low temperature lattice where the lowest Matsubara frequency is close to zero) this relation turns into

$$ma=\ln\left[\frac{1-6\kappa}{2\kappa}\right]\ . \tag{16}$$

The mass vanishes when $\kappa\to\frac{1}{8}$ as expected. Inverting this for κ gives

$$\kappa=\frac{1}{2\exp[ma]+6}\ , \tag{17}$$

which, for small masses, reduces to the naive relation,

$$\kappa=\frac{1}{2ma+8} \tag{18}$$

that one expects looking at the terms of the Lagrangian. For large lattices the lowest doubler mass becomes

$$ma_{\text{doubler}}=\lim_{\kappa\to1/8}\ln\left[\frac{1-2\kappa}{2\kappa}\right]=\ln[3]=1.098\,61\ . \tag{19}$$

For Kogut-Susskind fermions [12] the free propagator turns out to be a sum of two terms, having parts with an alternating sign in z direction. For Wilson fermions, with our choice of the source, the propagator is a single exponential, or hyperbolic cosine, on a finite lattice.

Furthermore, the sign of G_1 at $k=0$ changes at $\kappa_c=\frac{1}{8}$. Therefore, measuring the sign of the propagator can be used as an indicator of whether κ is effectively greater or less than κ_c.

One can infer from Eqs. (13)–(15) that the only effect of finite spatial lattice size is the discretization of the momenta. For a given momentum all lattice sizes give the same value of the screening mass. For a smaller lattice, the range of allowed momenta is more restricted, of course.

To be specific let us look at what happens with our lattice size: $8^2\times20\times4$. This is shown in Fig. 1. At κ_c the lowest momentum screening mass is at its minimum. If one increases κ the screening masses start to converge to a single value close to one at $\kappa=0.152$. At this point the dispersion relation is flat.

The sign of the propagator with this source depends on the momentum. Generally, the value of κ at which the sign changes increases with the momentum. For zero momentum it occurs at κ_c; for the smallest nonzero momentum in our lattice size it takes place at $\kappa=(2+\sqrt{2}-\sqrt{3})/11=0.1374$. The amplitude for the doubler does not change sign in this κ range.

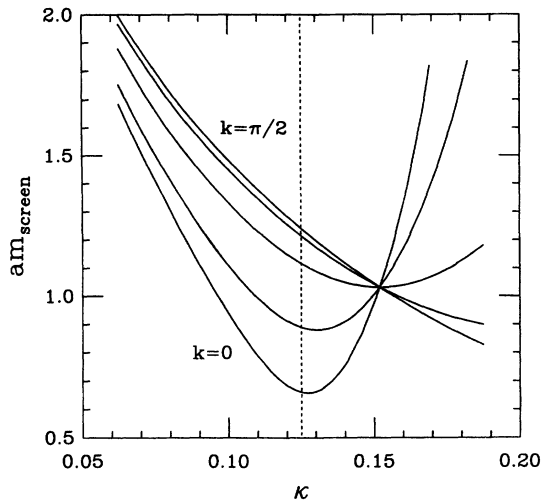

FIG. 1. The spatial screening mass at different spatial momenta for free Wilson fermions as a function of κ for an $8^2\times20\times4$ lattice. At $\kappa_c=\frac{1}{8}$ the higher masses are for higher momenta.

For our lattice size, inserting the appropriate momenta to Eq. (15) one obtains the following quark screening masses at $\kappa_c=\frac{1}{8}$:

$$\begin{aligned} &k=(0,0,0,\pi/4), \quad ma=0.6610\ , \\ &k=(\pi/4,0,0,\pi/4), \quad ma=0.8906\ , \\ &k=(\pi/2,0,0,\pi/4), \quad ma=1.1171\ , \\ &k=(3\pi/4,0,0,\pi/4), \quad ma=1.2149\ , \\ &k=(\pi,0,0,\pi/4), \quad ma=1.2411\ . \end{aligned} \tag{20}$$

For purely temporal momenta the free field screening mass is

$$\begin{aligned} &k=(0,0,0,\pm\pi/4), \quad ma=0.6610\ , \\ &k=(0,0,0,\pm3\pi/4), \quad ma=1.0711\ . \end{aligned} \tag{21}$$

Hence, the temporal doubler's screening mass is smaller than that of the spatial doubler.

III. SIMULATIONS AND RESULTS

Simulations were run on the Intel iPSC/860 and Paragon, and the nCUBE-2 at the San Diego Supercomputer Center, on the Thinking Machines Corporation CM5 at the National Center for Superconducting Applications, and on a cluster of RS6000 workstations at the University of Utah. We used the hybrid Monte Carlo algorithm with two flavors of dynamical quarks in all our simulations [13]. The parameters of our runs are listed in Tables I, II, and III.

For the $8^2\times20\times4$ runs we used trajectories with a length of one unit of simulation time and made measurements after every second trajectory. The step size for these runs ranged, in the normalization of Ref. [14], from 0.033 for the largest $6/g^2$ and smallest κ to 0.02 at the other extreme. Acceptance rates for these runs range from 70% to 90%, with an average over all the runs of 87%. For computation of the fermion force in the updating and the propagators in the measurements we used the conjugate gradient algorithm with even-odd incomplete lower upper (ILU) preconditioning [15]. The conjugate gradient residual, defined as $|\tilde{M}^\dagger\tilde{M}x-b|/|b|$ where $\tilde{M}$ is the preconditioned matrix, b is the source vector, and x is the solution vector, was 10^{-6}. Runs were made at $6/g^2=5.3$, 5.1, 5.0, and 4.9 with $N_t=4$. At $6/g^2=5.3$ we also made a series of runs with $N_t=6$. At $6/g^2=5.1$ we ran two points with $N_t=8$ and at $6/g^2=5.0$ two points with $N_t=6$. We also ran a series of simulations at $6/g^2=5.1$ on $6^2\times20\times4$ lattices to verify that the spatial size of the lattice was not seriously affecting our results.

TABLE I. Table of runs at fixed $6/g^2$ with varying κ. "(h)" and "(c)" indicate hot and cold starts.

N_t	$N_{x,y}$	$6/g^2$	κ	Traj.	Ignore	dt	Accept
4	8	4.9	0.180	650	100	0.02	0.88
4	8	4.9	0.181	320	100	0.02	0.94
4	8	4.9	0.182	810	100	0.02	0.90
4	8	4.9	0.1825	824(c)	100	0.02	0.86
4	8	4.9	0.1825	780(h)	100	0.02	0.88
4	8	4.9	0.183	624(h)	100	0.02	0.90
4	8	4.9	0.183	810(c)	600	0.02	0.87
4	8	4.9	0.184	610	100	0.02	0.93
4	8	5.0	0.173	540	100	0.025	0.86
4	8	5.0	0.175	500	100	0.02	0.92
4	8	5.0	0.177	400	100	0.02	0.90
4	8	5.0	0.178	474	100	0.02	0.94
4	8	5.0	0.180	630	100	0.02	0.92
4	8	5.0	0.182	256	100	0.02	0.86
6	8	5.0	0.175	240	80	0.02	0.94
6	8	5.0	0.180	360	60	0.0167	0.87
8	8	5.0	0.175	350	100	0.0167	0.91

At $6/g^2=5.3$ a series of short runs on $6^3\times4$ lattices was made for very large κ.

For reference we show a phase diagram for the relevant range of κ and $6/g^2$ in Fig. 2. Previous work showed that as κ increased from 0.16 to 0.19 along the $N_t=4$ high temperature crossover line the pion mass decreased, suggesting a closer approach to the high temperature transition in the chiral limit [3]. More recent work by Iwasaki *et al.*, beginning from the $6/g^2=0$ limit, suggested that a high temperature transition for zero quark mass might be found at $\kappa\approx0.225$ [16]. We have done a series of runs on $8^3\times4$ lattices in which we varied $6/g^2$ at $\kappa=0.20$, 0.21, and 0.22 to extend the previous work. As expected, the number of conjugate gradient iterations required in the updating increases as κ increases in this range, and the size of the possible updating time step decreases. Thus these runs have limited statistics. In Fig. 3 we show the plaquette and Polyakov loop as a function of $6/g^2$ for the various values of κ. Notice that the transition appears to be sharpest at $\kappa\approx0.19$, becoming smoother for larger and smaller κ. Even in those cases where the transition is very abrupt, we do not see the sorts of meta-

TABLE II. Table of runs at fixed $6/g^2$ with varying κ. "(*h*)" and "(*c*)" indicate hot and cold starts. Most of the $N_t=4$ runs were on $8^2\times20\times4$ lattices. The run indicated with a † at $\kappa=0.168, 6/g^2=5.3$ was done on a $8^2\times40\times4$ lattice.

N_t	$N_{x,y}$	$6/g^2$	κ	Traj.	Ignore	dt	Accept
4	8	5.1	0.165	1120	100	0.025	0.89
4	8	5.1	0.167	2660	100	0.025	0.89
4	8	5.1	0.169	460	100	0.025	0.87
4	8	5.1	0.170	700	100	0.025	0.90
4	8	5.1	0.171	980	100	0.025	0.89
4	8	5.1	0.172	3380	100	0.025	0.87
4	8	5.1	0.173	500	100	0.025	0.85
4	8	5.1	0.175	460	100	0.025	0.86
4	8	5.1	0.177	1800	100	0.025	0.88
4	8	5.1	0.179	660	100	0.025	0.88
4	6	5.1	0.169	860	200	0.0333	0.82
4	6	5.1	0.170	1000	100	0.0333	0.85
4	6	5.1	0.717	1360	100	0.0333	0.81
4	6	5.1	0.172	1120	100	0.0333	0.83
4	6	5.1	0.175	720	100	0.0333	0.81
8	8	5.1	0.167	512	100	0.025	0.82
8	8	5.1	0.173	279	100	0.02	0.87
8	8	5.1	0.177	440	100	0.02	0.66
4	8	5.3	0.155	2400	100	0.0333	0.78
4	8	5.3	0.157	660	100	0.0333	0.76
4	8	5.3	0.158	1239	100	0.0333	0.89
4	8	5.3	0.159	660	100	0.0333	0.89
4	8	5.3	0.160	1777	100	0.025	0.88
4	8	5.3	0.161	480	100	0.025	0.88
4	8	5.3	0.162	480	100	0.025	0.83
4	8	5.3	0.163	680	100	0.025	0.87
4	8	5.3	0.164	460	100	0.025	0.90
4	8	5.3	0.165	720	100	0.025	0.88
4	8	5.3	0.166	660	100	0.025	0.87
4	8	5.3	0.167	912	100	0.025	0.86
4	8	5.3	0.168	540	100	0.025	0.89
4†	8	5.3	0.168	840	100	0.025	0.80
4	8	5.3	0.169	380	100	0.025	0.86
4	8	5.3	0.170	380	100	0.025	0.79
4	8	5.3	0.172	440	100	0.025	0.87
6	12	5.3	0.155	320	100	0.0177	0.88
6	12	5.3	0.160	552	60	0.0177	0.91
6	12	5.3	0.165	666	216	0.0177	0.85
6	12	5.3	0.166	1403	400	0.0177	0.84
6	12	5.3	0.167	760	302	0.0177	0.84
6	12	5.3	0.168	603	200	0.0177	0.85

stability and tunneling characteristic of strong first order transitions. We do find cases where equilibration takes a long time. The worst case was in the run at $6/g^2=4.9$ and $\kappa=0.1825$. In this case we have plotted two points, from hot and cold starts. These points are marked by arrows in Fig. 3. However, these two runs eventually converged to similar values, lying in between the values in the early parts of the runs. The time history of the Polyakov loop in these two runs is shown in Fig. 4.

We now examine the $8^2\times20\times4$ runs in more detail. Figure 5 shows the real part of the Polyakov loop as a function of κ for the different values of $6/g^2$. For $6/g^2=5.3$ we also include values for $N_t=6$ to show how the transition point moves as N_t increases. For all of these values of $6/g^2$ we see the expected sharp increase in the Polyakov loop at a value of κ less than κ_c, where κ_c is the value at which the squared pion mass vanishes on a zero temperature lattice. We estimate κ_c at these values of $6/g^2$ from published values of κ_c in Refs. [7] and [4] and a recent measurement at $6/g^2=5.3$ by the HEMCGC group: $\kappa_c(5.3)=0.16794$ [17]. From a quadratic fit to these values, shown by a line in Fig. 2, we find $\kappa_c(6/g^2)=0.1687(2)$ at 5.3, 0.1795(4) at 5.1, 0.1861(12) at 5.0, and 0.1941(40) at 4.9.

Although not a physical quantity, the number of conjugate gradient iterations used in solving $\tilde{M}^\dagger\tilde{M}x=b$ indicates how singular $\tilde{M}$ is on the average. This quantity has been used as a probe of the physics in Ref. [16]. In Fig. 6 we show the average number of conjugate gradient iterations used in an updating step, where a linear extra-

TABLE III. Table of runs at fixed κ with varying $6/g^2$. "(h)" "(c)" indicate hot and cold starts. The acceptance rate gives the average over all runs in the sample kept for measurement, whether or not dt was changing during the runs.

N_t	$N_{x,y,z}$	$6/g^2$	κ	Traj.	Ignore	dt	Accept
4	8	4.75	0.19	578	100	0.014 286	0.912(13)
4	8	4.755	0.19	1504	750	0.014 286	0.960(6)
4	8	4.76(c)	0.19	837	500	0.014 286	0.948(11)
4	8	4.76(h)	0.19	362	100	0.014 286	0.962(12)
4	8	4.32	0.20	156	50	0.02	0.83(4)
4	8	4.36	0.20	172	50	0.02	0.83(3)
4	8	4.40	0.20	188	50	0.02	0.79(3)
4	8	4.44	0.20	152	50	0.02	0.77(4)
4	8	4.48	0.20	368	50	0.02	0.69(3)
4	8	4.50	0.20	244	100	0.014 286	0.84(3)
4	8	4.52	0.20	841	150	0.014 286	0.773(16)
4	8	4.54	0.20	566	150	0.014 286	0.72(2)
4	8	4.56	0.20	1324	200	0.014 286	0.941(7)
4	8	4.60	0.20	365	50	0.014 286	0.937(14)
4	8	4.64	0.20	244	50	0.02	0.959(14)
4	8	4.10	0.21	74	50	0.01	0.79(8)
4	8	4.20	0.21	267	50	0.005	0.90(2)
4	8	4.26	0.21	586	100	0.005	0.85(2)
4	8	4.28	0.21	478	100	0.005→0.0025	0.82(2)
4	8	4.30	0.21	454	100	0.005	0.904(16)
4	8	4.32	0.21	227	50	0.005	0.94(2)
4	8	4.34	0.21	259	50	0.007 143	0.943(15)
4	8	4.36	0.21	281	100	0.0025→0.007 143	0.960(14)
4	8	4.40	0.21	197	50	0.0025→0.01	0.95(2)
4	8	4.44	0.21	249	50	0.007 143→0.01	0.977(9)
4	8	4.50	0.21	120	50	0.05→0.01	0.94(3)
4	8	3.80	0.22	59	15	0.001	0.93(4)
4	8	3.90	0.22	56	30	0.002→0.0004	0.69(9)
4	8	3.96	0.22	39	25	0.002→0.0005	0.36(13)
4	8	4.00	0.22	119	80	0.004→0.002	0.50(8)
4	8	4.04	0.22	161	50	0.004	0.71(4)
4	8	4.06	0.22	119	40	0.003 333	0.78(5)
4	8	4.10	0.22	234	50	0.005	0.86(3)
4	8	4.20	0.22	90	50	0.007 143	0.98(3)
4	8	4.30	0.22	58	50	0.005→0.007 143	1.00(0)
4	8	4.40	0.22	90	50	0.01	0.95(3)
4	8	4.50	0.22	122	50	0.01→0.02	0.96(2)

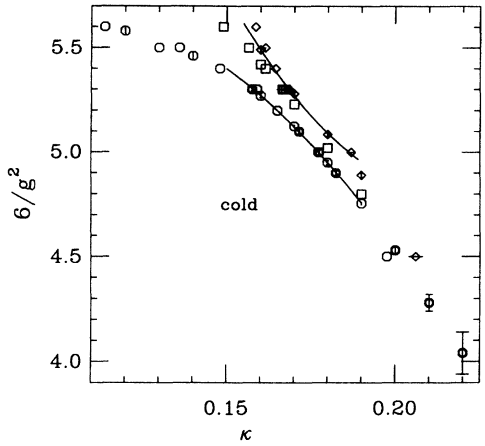

FIG. 2. Phase diagram showing estimates for the high temperature transition and κ_c. Circles represent the high temperature transition or crossover for $N_t=4$, squares the high temperature transition for $N_t=6$, and diamonds the zero temperature κ_c. Previous work included in this figure is from Refs. [2,6,7,3,4]. We show error bars where they are known. For series done at fixed κ the error bars are vertical, while for series done at fixed $6/g^2$ the bars are horizontal. Points coming from this work are shown in heavier symbols. The solid lines are fits to κ_t for $N_t=4$ and to κ_c used in interpolating and extrapolating.

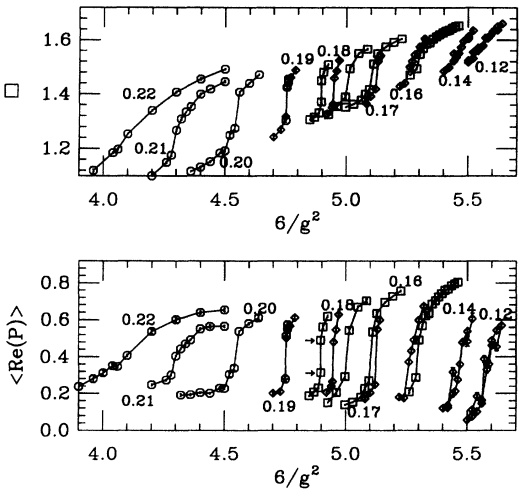

FIG. 3. The plaquette and Polyakov loop as a function of $6/g^2$ for various values of κ. The diamonds are previous results of Ref. [3] for $\kappa=0.12$, 0.14, 0.16, 0.17, 0.18, and 0.19. For $\kappa=0.12$ and 0.14 data from long runs as well as some data from short runs collected while generating hysteresis loops are shown. The octagons at $\kappa=0.20$, 0.21, and 0.22, are new results from $8^3\times4$ lattices. The squares come from runs on $8^2\times20\times4$ lattices. These runs were done at fixed values of $6/g^2$ with varying κ. They have been mapped onto this figure by fitting the $6/g_t^2,\kappa_t$ line (with a fit shown as a line in Fig. 2), and moving the points in the $\kappa,6/g^2$ plane parallel to this line. Specifically, we plot the points at $6/g^2_{\text{effective}}=6/g^2_{\text{run}}-\partial(6/g_t^2)/\partial\kappa_t(\kappa_{\text{run}}-\kappa_t)$. The fit for κ_t at $6/g^2=5.3$, 5.1, 5.0, and 4.9 is 0.1579, 0.1713, 0.1772, and 0.1827, respectively.

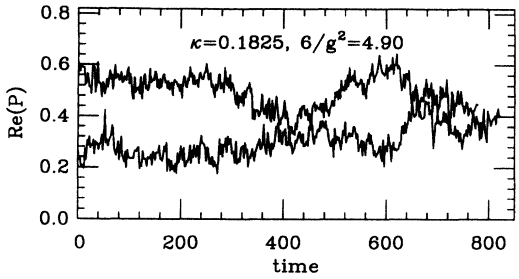

FIG. 4. Time history of the real part of the Polyakov loop for runs with hot and cold starts at $6/g^2=4.9$ and $\kappa=0.1825$.

polation of the last two time steps was used to produce a starting guess for the solution vector. For $6/g^2=5.3$ and $N_t=4$ there is very little effect on the number of iterations at κ_t. As $6/g^2$ is decreased for $N_t=4$ there is an increasingly sharp peak in the number of iterations at κ_c. Notice also the sharp peak in the $N_t=6$ results for $6/g^2=5.3$.

Figure 7 shows the average plaquette in these runs. Our normalization is such that the plaquette is three for a lattice of unit matrices. The plaquette also shows a sharp rise as the high temperature crossover is passed. Notice that for $6/g^2=5.3$ we have results for $N_t=4$ and 6 showing that this increase is in fact due to the time size of the lattice, or the temperature.

The chiral condensate $\bar{\psi}\psi$ is less useful for Wilson

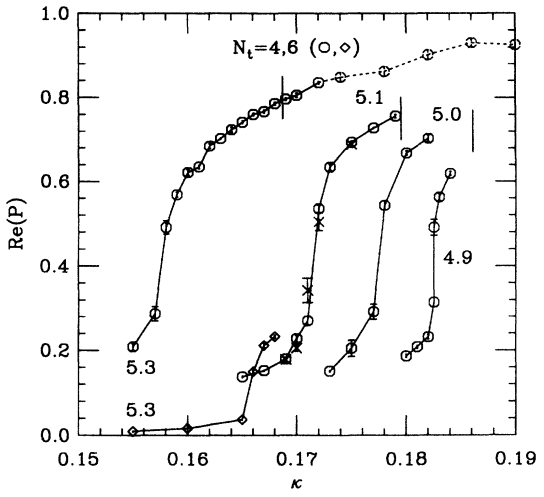

FIG. 5. Expectation value of the Polyakov loop as a function of κ for the various values of $6/g^2$. Results are shown for $N_t=4$ for $6/g^2=5.3$, 5.1, 5.0, and 4.9 (octagons). For $6/g^2=5.3$ we also show results for $N_t=6$ (diamonds). The crosses along the $6/g^2=5.1$ line are results on a $6^2\times24\times4$ lattice at $6/g^2=5.1$, to show that the spatial size of the lattice is not greatly affecting the results. The dotted symbols extending the $6/g^2=5.3$ line are short runs on a $6^3\times4$ lattice, showing that the behavior is smooth out to very large κ. The vertical lines mark the zero temperature κ_c for $6/g^2=5.2$, 5.1, and 5.0, respectively. [For $6/g^2=4.9$, $\kappa_c(T=0)\approx0.194$.]

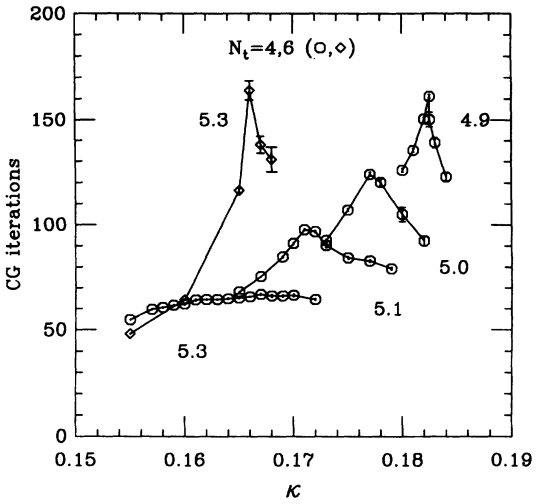

FIG. 6. Conjugate gradient iterations for updating step, as a function of κ for the various values of $6/g^2$. Again the diamonds are $N_t=6$ results at $6/g^2=5.3$.

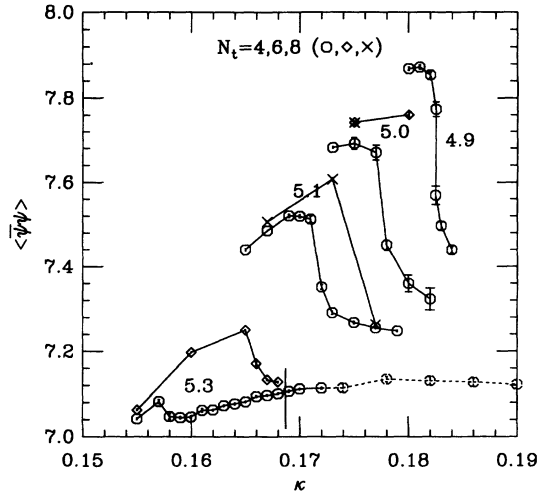

FIG. 8. Expectation value of $\bar{\psi}\psi$ as a function of κ for the various values of $6/g^2$. The dotted symbols for $6/g^2=5.3$ are short runs on a $6^3\times4$ lattice extending to κ far beyond the zero temperature κ_c shown by the vertical line.

quarks than for Kogut-Susskind quarks, since it does not go to zero in the high temperature phase without difficult subtractions. Nevertheless we plot it in Fig. 8. There is a clear drop in $\bar{\psi}\psi$ as the high temperature transition is crossed. This drop increases dramatically as $6/g^2$ decreases.

Perhaps the most physically relevant observable is the entropy. In Fig. 9 we plot $T\times s$ in units of a^{-4}. To give an idea of the normalization of this graph, for eight gluons in free field theory on an $8\times8\times20\times4$ lattice the gluon entropy would be $Ts_{\text{glue,free}}=0.040a^{-4}$, while for two flavors of free Wilson quarks at $\kappa=\kappa_c=0.125$ the entropy would be $Ts_{\text{quark,free}}=0.125a^{-4}$. The effects of the lattice spacing and spatial size are very large here; in the continuum with infinite spatial extent these numbers are 0.027 and 0.036, respectively. Strangely, when we divide the entropy into gauge and fermion parts as in Eqs. (2) and (3) we find that the gauge entropy is comparable to the fermion entropy instead of much smaller as would be the case with free fields on a lattice of this size.

The quark mass defined by the divergence of the axial pion propagator is plotted in Fig. 10. When this quark mass was small we had great difficulty in getting good fits to the forms in Eqs. (8) and (9). This is expected, because when the quark mass is small the amplitude for the prop-

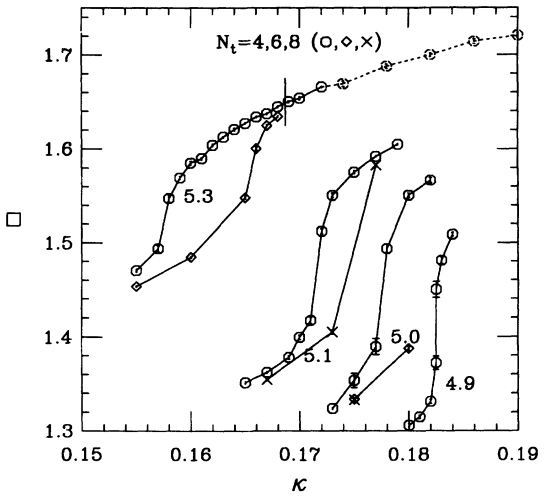

FIG. 7. Expectation value of the plaquette as a function of κ for the various values of $6/g^2$. Here we included values for larger N_t to emphasize the effect of the temperature. The dotted symbols for $6/g^2=5.3$ are short runs on a $6^3\times4$ lattice extending to κ far beyond the zero temperature κ_c shown by the vertical line.

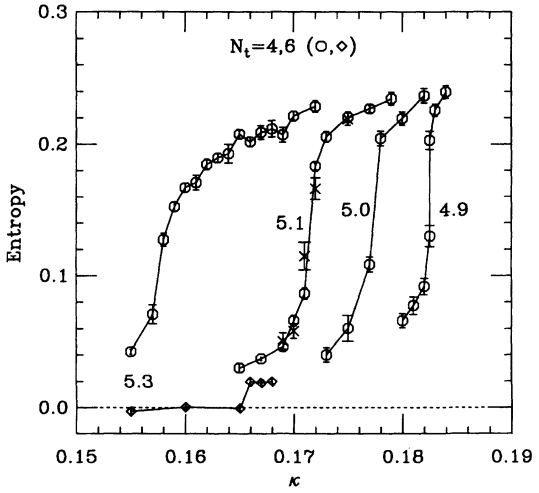

FIG. 9. Entropy (actually $T\times sa^4$) as a function of κ for the various values of $6/g^2$. Again we show the $6^2\times24\times4$ results for comparison.

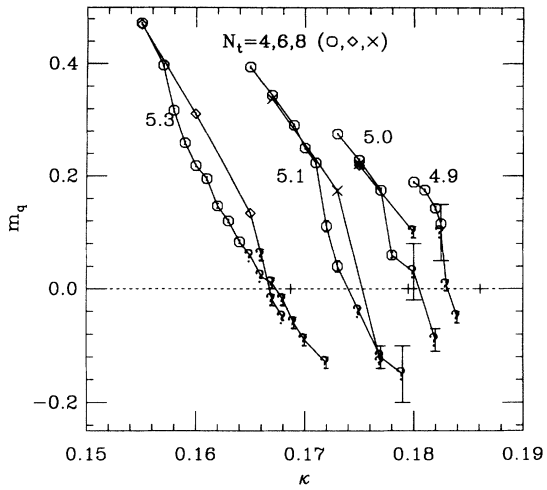

FIG. 10. Quark mass from the axial current as a function of κ for the various values of $6/g^2$. Points marked with question marks indicate runs where we were unable to get consistent fits as a function of distance. The plus signs on the $m_q=0$ line are the zero temperature κ_c for $6/g^2=5.3$, 5.1, and 5.0.

agator $A(z)$ is very small. Additionally, there is a tendency for the effective quark mass, or the quark mass coming from a fit over a short distance range, to increase with distance from the source. In cases where we were unable to get a fit with a satisfactory χ^2 or where the quark mass was not convincingly independent of distance, we plot the point with a question mark in Fig. 10. To pursue this further we ran one of the difficult points, $6/g^2=5.3$ and $\kappa=0.168$, on a $8^2\times40\times4$ lattice, allowing us to measure the ratio out to a distance of 20. Figure 11 summarizes the results. In this figure we show the effective pion mass obtained from $\Pi(x)$ and $A(z)$ by fitting to two successive distances, and the quark mass obtained from simultaneously fitting both propagators at the two successive distances (a one degree of freedom fit). Unfortunately, in all other cases the lattice was only 20 sites long and we have to draw conclusions from distances less than ten. In Fig. 10 we see that when the $N_t=4$ lattice enters the high temperature regime the pointlike axial current quark mass no longer agrees with the low temperature lattices ($N_t=6$ and 8). The plusses at $m_q=0$ in Fig. 10 are estimates for the zero temperature κ_c. The axial current quark masses go through zero at κ less than the zero temperature κ_c. When the axial current quark mass vanishes, the system is in the high temperature phase for $\beta>5.0$, while at $\beta=4.9$ k_t appears to coincide with the point where the axial current quark mass vanishes, within experimental uncertainty. Note, however, that the pion screening mass in the confinement phase is still nonzero at the transition point at $\beta=4.9$.

In Fig. 12 we show the squared pion screening masses in these runs. Again we see an increasingly sharp dip at κ_t as $6/g^2$ decreases and κ increases. The appearance of the cusp at $\beta=5.1$ coincides with the beginning of the region where the transition is abrupt. Screening masses for the π, ρ, σ, and a_1 mesons are shown in Figs. 13, 14, and 15. In all cases we see the screening masses coming together as the high temperature transition is crossed. However, we do not see any indication that the $\pi-\sigma$ or $\rho-a_1$ splittings in the high temperature regime are decreasing as $6/g^2$ decreases. Although the smaller pion masses in the cold regime suggest that chiral symmetry is being approached as we move toward smaller $6/g^2$ along the κ_t line, we do not see this trend in the high temperature screening masses. Also notice that there are nonzero splittings between the parity partners at the points where the axial current quark mass is zero. Thus the vanishing of this quark mass is not an indicator for complete chiral

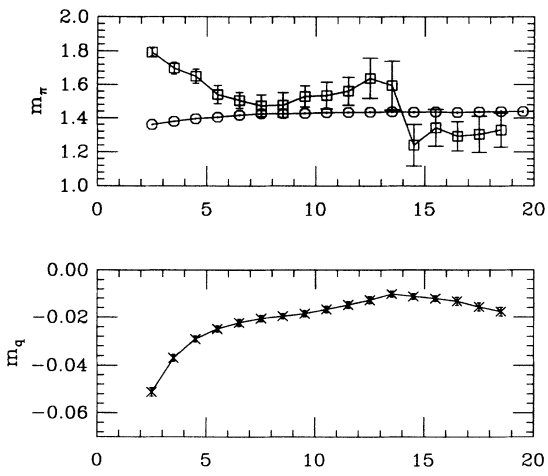

FIG. 11. Pion effective screening masses from $\Pi(z)$ (circles) and from $A(z)$ (squares), and the effective quark screening mass from their ratio. The results are from an $8^2\times40\times4$ lattice with $6/g^2=5.3$ and $\kappa=0.168$.

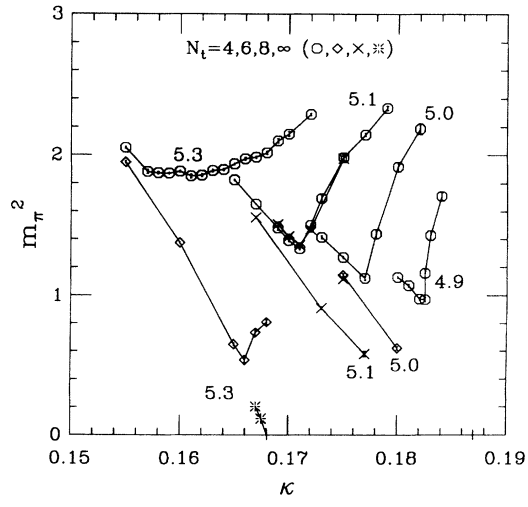

FIG. 12. Pion screening mass squared as a function of κ for the various values of $6/g^2$. Again, the circles are for $N_t=4$, the diamonds for $N_t=6$, and the crosses for $N_t=8$. The bursts are zero temperature pion masses from the HEMCGC Collaboration at $6/g^2=5.3$.

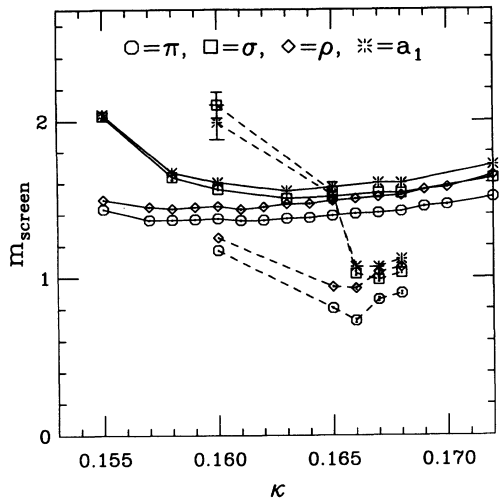

FIG. 13. Meson screening masses for $6/g^2=5.30$. The points connected by solid lines are for $N_t=4$ and the points connected by dashed lines for $N_t=6$.

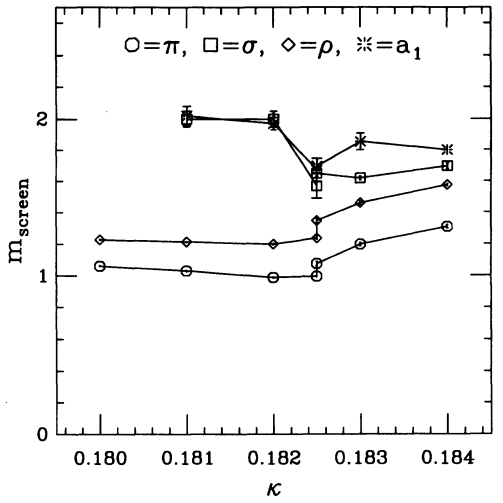

FIG. 15. Meson screening masses for $6/g^2=4.90$ at $N_t=4$. The two points at $\kappa=0.1825$ are from cold and hot starts.

symmetry restoration in the system.

To investigate the contributions of the doublers to thermodynamic quantities such as the entropy we measured the effective masses from the quark propagator in Landau gauge at a few values of κ and $6/g^2$. We find that fitting the quark screening propagators is more difficult than fitting the meson propagators. In part this is because the quark propagators fluctuate more from configuration to configuration. There also seems to be a systematic trend toward larger effective quark masses at larger distances. With these caveats, the masses of the physical quark and the lightest doublers are given in Table IV. The fits were selected by choosing the largest fit range that gives an acceptable confidence level. The ranges and confidence levels are also given in Table IV.

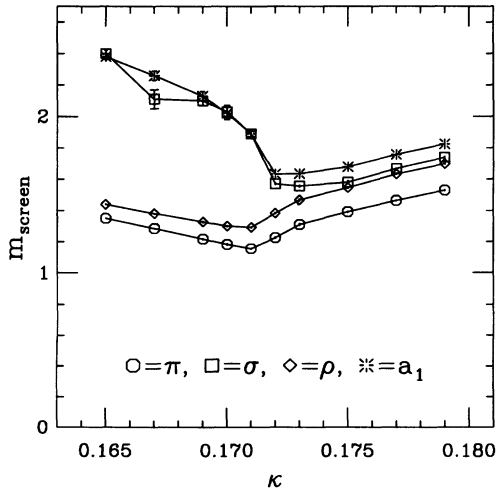

FIG. 14. Meson screening masses for $6/g^2=5.10$ at $N_t=4$.

IV. CONCLUSIONS

The most naive expectation regarding the thermodynamics of two flavors of Wilson quarks at fixed N_t is that there would be a line in the κ,β plane at which a confinement-deconfinement transition occurs, that the transition would be smooth (crossover or second order), that the pion mass would smoothly decrease along that line, and that at some point, possibly corresponding to the point where the transition line crossed the zero temperature $\kappa_c-\beta$ line, the pion mass would go to zero. At that point one would have a finite temperature confinement-deconfinement or chirally restoring transition analogous to that seen in staggered fermions. Simple arguments [9] would put this point around $\beta=5.0$ at $N_t=4$.

These naive expectations are not borne out by the data. The chiral limit is reached at a very small β value if it is reached at all. However, near $\beta=5.0$, $N_t=4$ Wilson thermodynamics displays a number of features which have no analogs in staggered fermion systems. The transition becomes very sharp, though not first order as far as we can tell. A cusp in the pion screening mass appears as one crosses from the confined to the deconfined phase. The axial vector quark mass becomes strongly N_t dependent at this point and for small N_t does not go to zero at its zero temperature κ value (at fixed β). The sharp transition persists down to $\beta=4.5,\kappa=0.20$ or so, at which point it once again becomes smooth. As far as we can tell, the zero temperature $\kappa=\kappa_c$ point plays no role in any $N_t=4$ effects we have observed.

It is tempting to speculate that the crossover line in the $\kappa,6/g^2$ plane is close to some phase boundary where the transition is steepest. We are currently exploring this region with $N_t=6$, where preliminary results indicate a change in the nature of the high temperature transition around this value of κ.

Indicators for the nature of the high temperature phase

TABLE IV. The screening masses for the quark and the lightest doublers. $\Delta ma_{s(t)}$ is the difference of the spatial (temporal) doubler screening mass to the quark screening mass at the lowest momenta. The sign is for $G(k_t=\pi/4)$. The fits were done simultaneously to all three propagators taking into account the cross correlations. The confidence level q and the range of each fit is also displayed.

N_t	κ	β	Sign	$ma(0,\pi/4)$	$ma(\pi,\pi/4)$	$ma(0,3\pi/4)$	Δma_s	Δma_t	q	Range
4	0.165	5.10	+	1.13(4)	2.3(4)	1.8(2)	1.1(4)	0.7(2)	0.47	3–10
4	0.167	5.10	+	1.13(4)	2.4(5)	1.8(3)	1.3(5)	0.6(3)	0.14	3–10
4	0.172	5.10	+	0.97(16)	1.5(3)	1.5(2)	0.5(3)	0.6(4)	0.43	4–10
4	0.177	5.10	−	1.05(9)	1.28(15)	1.33(11)	0.23(19)	0.27(15)	0.69	4–8
4	0.155	5.30	+	1.06(2)	1.63(13)	1.65(11)	0.57(13)	0.60(11)	0.68	3–9
4	0.160	5.30	+	0.89(4)	1.38(9)	1.22(5)	0.49(9)	0.34(7)	0.84	3–10
4	0.167	5.30	−	0.92(6)	1.51(9)	1.36(7)	0.59(11)	0.44(10)	0.57	3–9

give a somewhat mixed picture. It is clear from the meson screening masses and from $\bar{\psi}\psi$ that chiral symmetry is at least partially restored at high temperature. While the axial current quark mass goes to zero the $\pi-\sigma$ and $\rho-a_1$ splittings in the screening masses remain nonzero. Quark propagators in the Landau gauge suggest a large constituent quark mass at the transition, at least for $6/g^2=5.3$ and 5.1. This is consistent with earlier work [3] where at the $N_t=4$ crossover point near these (β,κ) values the zero temperature pion was found to be quite heavy.

Notice that the series of runs at $6/g^2=5.3$ extends to κ significantly larger than the zero temperature κ_c, and there is no noticeable effect on any of the measured quantities when this κ_c is crossed. (In fact, we have done short runs on $8^3\times4$ lattices for κ as large as 0.19 at $6/g^2=5.3$ and seen no effects.) The sign of the propagator of the zero momentum quark, shown in Table IV, is consistent with the sign of the axial current quark mass. Both of these quantities are behaving in the way one would expect in a free field theory at $\kappa>\kappa_c$.

ACKNOWLEDGMENTS

These calculations were carried out on the iPSC/860, the Paragon and the nCUBE-2 at the San Diego Supercomputer Center, on the CM5 at the National Center for Supercomputing Applications, on 15 IBM/RS6000 workstations in the Physics Department at the University of Utah, on an IBM/RS6000 cluster at the Utah Supercomputing Institute and on our local workstations. We are grateful to the staffs of these centers for their help. We also thank Tony Anderson and Reshma Lal of Intel Scientific Computers for their help with the Paragon. We would like to thank Akira Ukawa and Frithjof Karsch for helpful discussions. Several of the authors have enjoyed the hospitality of the Institute for Nuclear Theory, the Institute for Theoretical Physics, and the UCSB Physics department, where parts of this work were done. This research was supported in part by Department of Energy Grants Nos. DE-2FG02-91ER-40628, DE-AC02-84ER-40125, DE-AC02-86ER-40253, DE-FG02-85ER-40213, DE-FG03-90ER-40546, DE-FG02-91ER-40661, and National Science Foundation Grants Nos. NSF-PHY90-08482, NSF-PHY93-09458, NSF-PHY91-16964, NSF-PHY89-04035, and NSF-PHY91-01853.

APPENDIX

Expressions for the energy, pressure, and $\bar{\psi}\psi$ are found by differentiating the partition function with respect to $1/T$, volume, and quark mass, respectively. First, we write the action with adjustable lattice spacings in all directions. Introducing dimensionless parameters α_μ, we write the lattice spacing in the μ direction as $a_\mu=a\alpha_\mu$. Clearly this is redundant, since we have five parameters a and α_μ to specify four lattice spacings, but it is convenient and symmetric. In the conventional notation of Karsch, $\xi=\alpha_i/\alpha_t$, where all the spatial α's are the same. When we are done taking derivatives, all the α_μ will be set to one.

The partition function is

$$Z=\int [dU]e^{S_g+S_f} \tag{A1}$$

where the gauge action is

$$S_g=\sum_x \sum_{\mu>\nu} \frac{2}{g_{\mu\nu}^2}\frac{\alpha_x\alpha_y\alpha_z\alpha_t}{\alpha_\mu^2\alpha_\nu^2}\Box_{\mu\nu} \tag{A2}$$

where $\Box_{\mu\nu}$ is the plaquette in the $\mu\nu$ plane normalized to three for unit matrices. We allow a different gauge coupling $g_{\mu\nu}$ in each plane. The fermion action is

$$S_f=\frac{n_f}{2}\mathrm{Tr}\ln M^\dagger M \tag{A3}$$

where

$$M=1-\kappa\sum_\mu \frac{\epsilon_\mu}{\alpha_\mu}\not{D}_\mu \tag{A4}$$

where

$$\not{D}_\mu=(1+\gamma_\mu)U_\mu(x)\delta_{y,x+\hat{\mu}}+(1-\gamma_\mu)U_\mu^\dagger(x-\hat{\mu})\delta_{y,x-\hat{\mu}}\ . \tag{A5}$$

The α_μ in the coefficient of $\not{D}_\mu$ takes care of the dimensional scaling of the first derivative. Notice that we have made a somewhat arbitrary choice in M when we scaled the irrelevant second derivative part with α_μ in the same way that we scaled the first derivative part. The ϵ_μ in the coefficient must be adjusted to get correlation functions to be Euclidean invariant. Its role is similar to the

Karsch coefficients C_σ and C_τ in the gauge action. Presumably ϵ_μ has a power series expansion in g just as C_σ and C_τ. Once again we have more parameters than we need: four ϵ_μ and κ for four directions. This parametrization is convenient because it includes the customary κ and, later, κ_c as parameters. We can fix the ambiguity well enough for our purposes by requiring that $\epsilon_\mu=1$ when all the α_μ are equal. In other words, if all directions are scaled by the same factor the only thing that changes is κ.

Let κ_c be the value of κ at which the pion mass and quark mass vanish, at least on an infinite lattice. Following free field theory, we introduce a quark mass

$$2ma=\kappa^{-1}-\kappa_c^{-1} \tag{A6}$$

so that

$$M=\frac{1}{\kappa_c^{-1}+2ma}\left[2ma+\kappa_c^{-1}-\sum_\mu \frac{\epsilon_\mu}{\alpha_\mu}\not{D}_\mu\right] . \tag{A7}$$

Here κ_c^{-1} will be a function of the couplings $g_{\mu\nu}$ and the scale factors α_μ. In free field theory, $\kappa_c^{-1}=2\sum_\mu \alpha_\mu^{-1}$. ($\epsilon_\mu=1$ in free field theory.)

We find the energy, pressure, and $\bar\psi\psi$ by differentiating the partition function:

$$\epsilon=-\frac{1}{V}\frac{\partial \ln Z}{\partial\beta}\bigg|_{V,m\ \text{const}} , \tag{A8}$$

$$p=\frac{1}{\beta}\frac{\partial \ln Z}{\partial V}\bigg|_{\beta,m\ \text{const}} , \tag{A9}$$

$$\bar\psi\psi=\frac{1}{\beta V}\frac{\partial \ln Z}{\partial m}\bigg|_{\beta,V\ \text{const}} . \tag{A10}$$

Here V is the volume, $V=a^3\prod_i N_i\alpha_i=a^3N_s^3\alpha_s^3$. β is the inverse temperature, $\beta=aN_t\alpha_t$. Here the energy and pressure derivatives are taken with m constant, rather than with κ constant. This is because κ_c depends on the α_μ, so that if we distort the lattice while holding κ fixed, the quark mass, and every physical mass, will vary sharply.

$$\frac{\partial}{\partial\beta}=\frac{1}{N_t a}\frac{\partial}{\partial\alpha_t} \tag{A11}$$

and

$$\frac{\partial}{\partial V}=\frac{1}{3N_s^3a^3\alpha_s^2}\frac{\partial}{\partial\alpha_s} . \tag{A12}$$

Alternatively, it may be easier to vary the volume by varying only one of the spatial lattice spacings

$$\frac{\partial}{\partial V}=\frac{1}{N_s^3a^3\alpha_x\alpha_y}\frac{\partial}{\partial\alpha_z} . \tag{A13}$$

The gauge energy and pressure are standard [18–20]. Following Ref. [18], we define two derivatives:

$$C_\sigma=-\frac{\partial g_{\mu\nu}^{-2}}{\partial\alpha_\lambda} \tag{A14}$$

where λ is not one of μ or ν and

$$C_\tau=-\frac{\partial g_{\mu\nu}^{-2}}{\partial\alpha_\lambda} \tag{A15}$$

where λ is one of μ or ν.

Because stretching both the time and space directions is equivalent to changing the lattice spacing, C_σ and C_τ are related to the β function:

$$\left[\sum_\mu \frac{\partial}{\partial\alpha_\mu}\right] g_{ab}^{-2}=-2C_\sigma-2C_\tau=\frac{\partial g^{-2}}{\partial \ln(a)} . \tag{A16}$$

The contributions to the energy and pressure from S_g and S_f add. Doing the differentiation, and then setting the α_μ to one, the gluon energy is

$$\epsilon_g a^4=\frac{1}{N_s^3N_t}\sum_x\left\langle\frac{6}{g^2}(\Box_{st}-\Box_{ss})+6C_\sigma\Box_{ss}+6C_\tau\Box_{st}\right\rangle . \tag{A17}$$

Here $\Box_{ss}$ and $\Box_{st}$ are the space-space and space-time plaquettes, again normalized to three for a lattice of unit matrices.

For the gluon pressure, we find

$$p_g a^4=\frac{1}{N_s^3N_t}\sum_x\left\langle\frac{2}{g^2}(\Box_{st}-\Box_{ss})-2C_\sigma(\Box_{ss}+2\Box_{st})-2C_\tau(2\Box_{ss}+\Box_{st})\right\rangle . \tag{A18}$$

We also consider the linear combination $\epsilon+p$, the entropy:

$$s_g a^4\frac{1}{aN_t}=\epsilon_g a^4+p_g a^4=\frac{1}{N_s^3N_t}\sum_x\left\langle\left[\frac{8}{g^2}+4(C_\tau-C_\sigma)\right](\Box_{st}-\Box_{ss})\right\rangle . \tag{A19}$$

The entropy is obviously zero at $T=0$.

Just as the gauge couplings vary with the lattice spacings, κ_c^{-1} and ϵ_μ vary with the lattice spacings as we try to hold m fixed. There is an explicit dependence of κ_c^{-1} on m plus a dependence of κ_c^{-1} on g, where g is varying with the α_μ. Now it clearly does not matter which direction we stretch the lattice, since κ_c^{-1} is defined on the infinite lattice, so

$$\frac{\partial\kappa_c^{-1}}{\partial\alpha_t}=\frac{\partial\kappa_c^{-1}}{\partial\alpha_x}\cdots . \tag{A20}$$

Therefore

$$\frac{\partial\kappa_c^{-1}}{\partial\alpha_s}\bigg|_{\alpha_\mu=1}=3\frac{\partial\kappa_c^{-1}}{\partial\alpha_t}\bigg|_{\alpha_\mu=1} . \tag{A21}$$

There are two independent derivatives of the ϵ_μ, analogous to C_σ and C_τ. Define

$$B_\tau = \frac{\partial \epsilon_\mu}{\partial \alpha_\mu} \tag{A22}$$

and

$$B_\sigma = \frac{\partial \epsilon_\mu}{\partial \alpha_\nu}, \quad \mu \neq \nu \; . \tag{A23}$$

To compute $\bar{\psi}\psi$ we can just set α_μ and ϵ_μ to one at the beginning:

$$a^3\bar{\psi}\psi = \frac{1}{N_s^3 N_t}\frac{N_f}{2}\left\langle \frac{\partial}{\partial ma} \operatorname{Tr} \ln M^\dagger M \right\rangle$$

$$= \frac{1}{N_s^3 N_t}\frac{N_f}{2}\left\langle \operatorname{Tr}\frac{1}{M^\dagger M}\left[\frac{\partial M^\dagger}{\partial ma}M + M^\dagger \frac{\partial M}{\partial ma}\right]\right\rangle$$

$$= \frac{1}{N_s^3 N_t}\frac{N_f}{2}\left\langle \operatorname{Tr}\left[\frac{1}{M^\dagger}\frac{\partial M^\dagger}{\partial ma} + \frac{1}{M}\frac{\partial M}{\partial ma}\right]\right\rangle . \tag{A24}$$

The two parts are complex conjugates, so keep only one and take twice the real part. Using Eq. (A7),

$$a^3\bar{\psi}\psi = \frac{1}{N_s^3 N_t}\frac{N_f}{2}\operatorname{Re}\left\langle \operatorname{Tr}\frac{1}{M^\dagger}\left[\frac{-2}{(\kappa_c^{-1}+2ma)^2}\left[2ma+\kappa_c^{-1}\sum_\mu \not{D}_\mu^\dagger\right]+2\left[\frac{1}{\kappa_c^{-1}+2ma}\right]\right]\right\rangle$$

$$= \frac{1}{N_s^3 N_t}\frac{4\kappa N_f}{2}\operatorname{Re}\left\langle \operatorname{Tr}\left[\frac{1}{M^\dagger}-1\right]\right\rangle , \tag{A25}$$

where in the last step we used $1/\kappa_c^{-1}+2ma=\kappa$. Looking at the derivation shows that the 1 in Eq. (A25) comes from differentiating the $1/\kappa_c^{-2}+2ma$ outside the parentheses in Eq. (A7). Had we taken the fermion matrix to be

$$M = \left[2ma+\kappa_c^{-1}-\sum_\mu \frac{\epsilon_\mu}{\alpha_\mu}\not{D}_\mu\right] , \tag{A26}$$

this term would be absent. Since this latter form is closer to the usual continuum Lagrangian, we prefer

$$\bar{\psi}\psi = \frac{1}{N_2^3 N_t}\frac{4\kappa N_f}{2}\operatorname{Re}\left\langle \operatorname{Tr}\frac{1}{M^\dagger}\right\rangle \tag{A27}$$

as our expression for $\bar{\psi}\psi$.

Now for the fermion energy, differentiate Eq. (A4) and then set α_μ and ϵ_μ to one:

$$\epsilon_f a^4 = \frac{-1}{N_s^3 N_t}\frac{N_f}{2}\left\langle 2\operatorname{Re}\operatorname{Tr}\frac{1}{M^\dagger}\frac{\partial M^\dagger}{\partial \alpha_t}\right\rangle$$

$$= \frac{-2}{N_s^3 N_t}\frac{N_f}{2}\operatorname{Re}\left\langle \frac{1}{M^\dagger}\left[\frac{-1}{(\kappa_c^{-1}+2ma)^2}\left[2ma+\kappa_c^{-1}-\sum_\mu \not{D}_\mu^\dagger\right]\frac{\partial \kappa_c^{-1}}{\partial \alpha_t}+\frac{1}{\kappa_c^{-1}+2ma}\left[\not{D}_0^\dagger-\sum_\mu \frac{\partial \epsilon_\mu}{\partial \alpha_t}\not{D}_\mu^\dagger+\frac{\partial \kappa_c^{-1}}{\partial \alpha_t}\right]\right]\right\rangle \tag{A28}$$

$$= \frac{2}{N_s^3 N_t}\frac{\kappa N_F}{2}\operatorname{Re}\left\langle \frac{\partial \kappa_c^{-1}}{\partial \alpha_t}\left[1-\frac{1}{M^\dagger}\right]-\frac{1}{M^\dagger}\left[\not{D}_0^\dagger-\beta_\tau \not{D}_0^\dagger-\sum_i B_\sigma \not{D}_i^\dagger\right]\right\rangle , \tag{A29}$$

where in the last step we used $1/\kappa_c^{-1}+2ma=\kappa$.

For the fermion pressure,

$$p_f a^4 = \frac{1}{3N_s^3 N_t}\frac{N_f}{2}\left\langle 2\operatorname{Re}\operatorname{Tr}\frac{1}{M^\dagger}\frac{\partial M^\dagger}{\partial \alpha_s}\right\rangle$$

$$= \frac{2}{3N_s^3 N_t}\frac{N_f}{2}\operatorname{Re}\left\langle \frac{1}{M^\dagger}\left[\frac{-1}{(\kappa_c^{-1}+2ma)^2}\left[2ma+\kappa_c^{-1}-\sum_\mu \not{D}_\mu^\dagger\right]\frac{\partial \kappa_c^{-1}}{\partial \alpha_c}\right.\right.$$

$$\left.\left.+\frac{1}{\kappa_c^{-1}+2ma}\left[\sum_i \not{D}_i-\sum_\mu \frac{\partial \epsilon_\mu}{\partial \alpha_s}\not{D}_\mu^\dagger+\frac{\partial \kappa_c^{-1}}{\partial \alpha_s}\right]\right]\right\rangle \tag{A30}$$

$$= \frac{-2}{3N_s^3 N_t}\frac{\kappa N_f}{2}\operatorname{Re}\left\langle \frac{\partial \kappa_c^{-1}}{\partial \alpha_s}\left[1-\frac{1}{M^\dagger}\right]+\frac{1}{M^\dagger}\left[3B_\sigma \not{D}_0^\dagger+(2B_\sigma+B_\tau)\sum_i \not{D}_i^\dagger-\sum_i \not{D}_i^\dagger\right]\right\rangle . \tag{A31}$$

Just as for $\bar{\psi}\psi$, the 1 term in ϵ_f and p_f comes from differentiating the overall factor of κ^{-1}. It can be included or not, as desired. It will cancel when the finite parts of the energy and pressure are calculated by subtracting the zero temperature result from the nonzero temperature result. However, the $(1/M^\dagger)(\partial\kappa_c^{-1}/\partial\alpha_t)$ term will not cancel out, since $\bar{\psi}\psi$ is temperature dependent. In practice $\langle \mathrm{Tr} 1/M^\dagger \rangle$ is fairly close to $\langle \mathrm{Tr} 1 \rangle = 4\times 3$, so numerically it may be best to leave the 1 in. Then we would use

$$1-\frac{1}{M^\dagger}=\frac{\kappa \not{D}^\dagger}{M^\dagger} \tag{A32}$$

to express the energy and pressure just in terms of the expectation values of the spatial and temporal components of $\not{D}^\dagger$.

Much of the difficulty cancels out if we look at the entropy, or sum of energy and pressure:

$$\begin{aligned} s_f a^4 \frac{1}{aN_t} &= \epsilon_f a^4 + p_f a^4 \\ &= \frac{-2}{N_s^3 N_t}\frac{\kappa N_f}{2}\,\mathrm{Re}\left\langle \mathrm{Tr}\frac{1}{M^\dagger}[1+(B_\tau - B_\sigma)] \right. \\ &\quad \left. \times \left[\not{D}_0 - \frac{1}{3}\sum_i \not{D}_i \right] \right\rangle . \end{aligned} \tag{A33}$$

The relation

$$\frac{\partial\kappa_c^{-1}}{\partial\alpha_s}=3\frac{\partial\kappa_c^{-1}}{\partial\alpha_t} \tag{A34}$$

resulted in all the derivative terms canceling. (Remember, by $\partial/\partial\alpha_s$ we mean $\partial/\partial\alpha_x+\partial/\partial\alpha_y+\partial/\partial\alpha_z$ vary all the spatial α_i together.) As usual, the entropy is obviously zero at $T=0$, where $\not{D}_i=\not{D}_0$. Since no zero temperature subtraction is required for the entropy, the terms involving B_τ and B_σ will be higher order in g^2 than the "1" term, and we have neglected them in Eq. (3).

Obviously, the big problem in getting the energy and pressure separately is to find $\partial\kappa_c^{-1}/\partial\alpha_\mu$ and B_τ and B_σ. From Euclidean invariance, $\partial\kappa_c^{-1}/\partial\alpha_\mu$ is independent of μ. The variable κ_c^{-1} depends on the α_μ in two ways. First, there is an "explicit" dependence. From examining the fermion matrix, Eq. (A4), we see that if all the α_μ are scaled together with g held fixed, κ_c is proportional to α. Thus

$$\left[\frac{\partial\kappa_c^{-1}}{\partial\alpha_\mu}\right]_{\text{explicit}}=\frac{-\kappa_c^{-1}}{4} . \tag{A35}$$

Secondly, there is an "implicit" dependence of κ_c^{-1} on α_μ coming from the fact that κ_c depends on g^{-2}, and we adjust the $g^2_{\mu\nu}$ as we adjust the α_μ. Again, Euclidean invariance says

$$\left[\frac{\partial\kappa_c^{-1}}{\partial\alpha_\mu}\right]_{\text{implicit}}=\frac{1}{4}\frac{\partial\kappa_c^{-1}}{\partial\ln(a)} , \tag{A36}$$

so only the β function appears:

$$\begin{aligned} \left[\frac{\partial\kappa_c^{-1}}{\partial\alpha_\mu}\right]_{\text{implicit}} &= \frac{1}{4}\frac{\partial\kappa_c^{-1}}{\partial\ln(a)} \\ &= \frac{1}{4}\frac{\partial\kappa_c^{-1}}{\partial 6/g^2}\frac{\partial 6/g^2}{\partial\ln(a)} . \end{aligned} \tag{A37}$$

We could proceed by estimating $\partial\kappa_c^{-1}/\partial 6/g^2$ from our data at various values of $6/g^2$, or from correlations of the hadron propagators with the plaquette. Similarly, we could take a β function either from perturbation theory or from some set of lattice simulations. We will not solve this problem here, so we will only quote the entropy rather than the energy and pressure separately.

[1] M. Fukugita, S. Ohta, and A. Ukawa, Phys. Rev. Lett. **57**, 1974 (1986).

[2] A. Ukawa, in *Lattice '88,* Proceedings of the International Symposium, Batavia, Illinois, 1988, edited by A. S. Kronfeld and P. B. Mackenzie [Nucl. Phys. B (Proc. Suppl.) **9**, 463 (1989)].

[3] HEMCGC Collaboration, K. M. Bitar *et al.*, Phys. Rev. D **43**, 2396 (1991).

[4] C. Bernard, T. A. DeGrand, C. DeTar, S. Gottlieb, A. Krasnitz, M. C. Ogilvie, R. L. Sugar, and D. Toussaint, Phys. Rev. D **46**, 4741 (1992).

[5] Y. Iwasaki, K. Kanaya, S. Sakai, and T. Yoshie, in *Lattice '92,* Proceedings of the International Symposium, Amsterdam, The Netherlands, 1992, edited by J. Smit and P. van Baal [Nucl. Phys. B (Proc. Suppl.) **30**, 327 (1993)]; in *Lattice '93,* Proceedings of the International Symposium, Dallas, Texas, 1993, edited by T. Draper *et al.* [Nucl. Phys. B (Proc. Suppl.) **34**, 314 (1994)].

[6] K. Bitar, A. D. Kennedy, and P. Rossi, Phys. Lett. B **234**, 333 (1990).

[7] R. Gupta, A. Patel, C. Baillie, G. Guralnik, G. Kilcup, and S. Sharpe, Phys. Rev. D **40**, 2072 (1989).

[8] K. Bitar *et al.*, in *Lattice '92* [5], p. 401.

[9] A. Hasenfratz and T. A. DeGrand, Phys. Rev. D **49**, 466 (1994).

[10] M. Bochicchio, L. Maiani, G. Martinelli, G. Rossi, and M. Testa, Nucl. Phys. **B262**, 331 (1985); L. Maiani and G. Martinelli, Phys. Lett. B **178**, 265 (1986).

[11] S. Itoh, Y. Iwasaki, Y. Oyanagi, and T. Yoshie, Nucl. Phys. **B274**, 33 (1986); Y. Iwasaki, L. Kanaya, S. Sakai, and T. Yoshie, Phys. Rev. Lett. **67**, 1494 (1991).

[12] G. Boyd, Sourendu Gupta, and F. Karsch, Nucl. Phys. **B385**, 481 (1992).

[13] S. Duane, A. D. Kennedy, B. J. Pendleton, and D. Roweth, Phys. Lett. B **195**, 216 (1987).

[14] S. Gottlieb, W. Liu, D. Toussaint, and R. L. Sugar, Phys. Rev. D **35**, 2531 (1987).

[15] T. DeGrand, Comput. Phys. Commun. **52**, 161 (1988); R. Gupta, A. Patel, C. Baillie, G. Guralnik, G. Kilcup, and S. Sharpe, Phys. Rev. D **40**, 2072 (1989); T. DeGrand and P. Rossi, Comput. Phys. Commun. **60**, 211 (1990).

[16] Y. Iwasaki, K. Kanaya, S. Sakai, and T. Yoshie, in *Lattice*

'91, Proceedings of the International Symposium, Tsukuba, Japan, 1991, edited by M. Fukugita *et al.* [Nucl. Phys. B (Proc. Suppl.) **26**, 311 (1992)]; Phys. Rev. Lett. **69**, 21 (1992).

[17] K. M. Bitar *et al.*, this issue, Phys. Rev. D **49**, 3546 (1994).

[18] F. Karsch, Nucl. Phys. **B205**, 285 (1982).

[19] J. Engels, F. Karsch, I. Montvay, and H. Satz, Phys. Lett. **101B**, 89 (1981); Nucl. Phys. **B205**, 545 (1982); T. Celik, J. Engels, and H. Satz, Phys. Lett. **129B**, 323 (1983).

[20] R. Trinchero, Nucl. Phys. **B227**, 61 (1983).